Modelling and analysis of crack turning on aeronautical structures

Llorenç Llopart Prieto

Modelling and analysis of crack turning on aeronautical structures

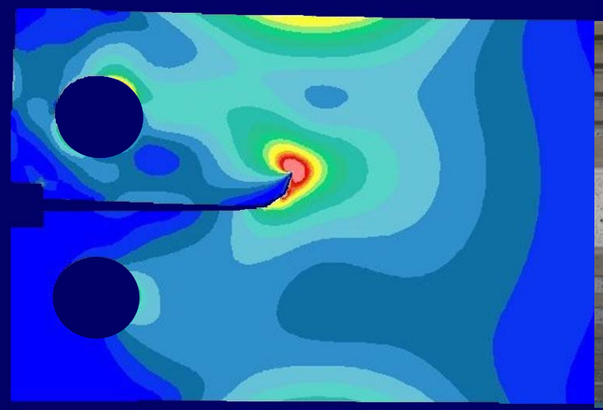

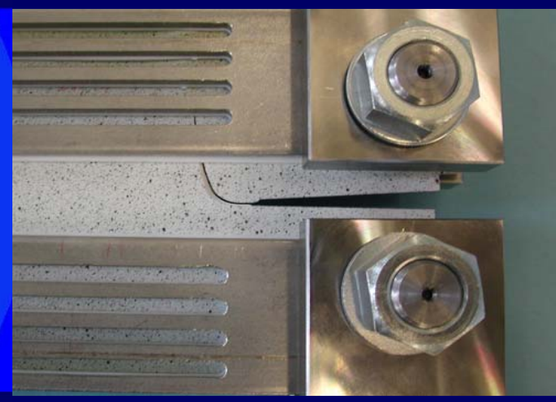

Doctoral Thesis

Llorenç Llopart Prieto

Director:
Dr. Marc Anglada i Gomila

Departament de Ciència dels Materials i Enginyeria Metal·lúrgica
UNIVERSITAT POLITÈCNICA DE CATALUNYA

Company director:
Elke Hombergsmeier

EADS
European Aeronautical Defence and Space company

EADS

UNIVERSITAT POLITÈCNICA DE CATALUNYA

Llorenç Llopart Prieto

Ottoburnn / Barcelona April 2007

5 Modelling tool for crack growth analysis

This chapter deals with the procedure followed in order to select and tune-up a simulation tool. First section defines the criteria applied to select a modelling tool. The second one introduces the screened commercial and non-commercial codes that are able to compute fracture mechanics parameters. The comparison among the different tools is presented here. The selection is done in section 5.3 and two of them are analysed in depth. A brief description of the implementation of the selected software is given in section 5.4. Finally, in section 5.5, the reliability of the purchased and implemented tool is tested by means of literature and experimental test data.

The screening of the different software was performed in the second quarter of 2002, but the capabilities of the tools were updated at the end of 2005, and most of them are continuously being developed and improved. Therefore, the latest state of each program can be checked by the given web pages in the references.

5.1 Selection conditions

As defined in section 3.1, the selected tool should be able to calculate at least K_I and K_{II} on two and three-dimensional models. It should have design facilities and it should be capable of being implemented. Finally, it must be “easy to use” in order to be a consulting tool for a common engineer. “Easy to use” denotes the minimisation of time costs spent on data preparation and interpretation of the results, that is:

a) the capability to generate quickly and easily *FEM* or *BEM* meshes,

b) the aptitude to enter material properties and boundary conditions in an easy way,

c) the support on performing modification and editing tasks promptly and conveniently,

d) and the skill to extract the results quickly and suitably.

5.2 Modelling tools

The development of *FE*-codes to conduct linear and non-linear stress analysis started in the 1970's. The first software which can compute both the *SIF* and the *J*-integral were ABAQUS®, ANSYS®, MSC/NASTRAN® and STAGS®.

A great number of software with different fracture mechanics capabilities have been developed since then. Due to this large number of tools, only the most interesting tools, congruent with the conditions defined above, were checked. At least, one tool for each method of analysis was treated (i.e. analytic, *FE* h- and p-element method and *BE*-method). The checked codes have been: NASGRO®/AFGROW® as analytic calculation codes, SAMCEF®, ABAQUS® and ANSYS® as finite h-element method codes, FRANC3D®, BEASY® and Crack-Kit® as boundary element method codes and StressCheck® as finite p-element method code. Differences between these methods have already been explained in section 2.3.

In the following only the tools which were directly used by the author are described. Details of other tools, also mentioned in this work, are given in the annexes A.4.

5.2.1 NASGRO®/AFGROW®

NASA GROwth code (NASGRO®) was developed at the National Aeronautics and Space Administration (*NASA*) in order to perform fracture analysis. Due to industrial-user interests a partnership with Southwest Research Institute® (*SwRI*) was developed. This formed and managed a consortium to provide guidance and support for NASGRO® development and user services.

The code NASGRO® is a collection of programs, which gives the possibility to analyse fatigue crack growth and fracture, to perform assessments of structural life, to process and store fatigue crack growth properties, to analyse fatigue crack initiation and to compute stresses.

On the other hand, Air Force GROWth crack prediction code (AFGROW®) is a code developed by the US Air force that it is based on NASGRO®.

These tools incorporate approximate solutions for *SIF*s and a database for material parameters, e.g. crack growth under corrosion conditions and material properties that are dependent on the orientation of the specimen with respect to the rolling direction. Both codes have approximate analytical solutions for the *SIF* of predefined specimen geometries. With these approximations and empirical models, e.g. Paris' law, the life of a specimen under different loading conditions, as constant amplitude or spectrum loading, can be evaluated [W1, W2].

5.2.2 ANSYS®

ANSYS® Mechanical™ is a simulation tool for product design and optimisation. The ANSYS family is a tool covering both the linear and non-linear analyses. The fatigue module can simulate cyclic loading conditions and supports stress and strain-based fatigue, constant amplitude, proportional loading and non-constant amplitude. The tool allows displaying on a contour plot fatigue life, damage, factor of safety, stress biaxiality, equivalent reversed stress and fatigue sensitivity. For the calculation of fracture mechanics problems, special crack front elements (collapsed quadrilaterals or hexahedrons) are available [W3].

5.2.3 FRANC3D®

FRacture ANalysis Code *3D* (FRANC3D®) is an analysis code especially designed for crack growth simulation at the Cornell University, Ithaca, USA. It contains several empirical laws and second order crack turning criteria. The user has to provide the geometry, the material properties (elastic or elasto-plastic) and the magnitude of the advanced crack per step. Through a linked database (NASGRO®) the program calculates the life cycles between two crack fronts using one of the implemented empirical laws, i.e. Paris, Forman-Newman-deKoning or SINH. The program needs a widely number of material inputs, which can be found by means of experimental results on each material system. However, it represents a substantial amount of work, but *NASA* had done it for over 300 different materials and environment combinations. These are incorporated into the NASGRO® and FRANC3D® codes [46, W4].

5.2.4 Crack-Kit®

Crack-Kit® is a *BEM*-tool developed at the European Aeronautics Space and Defence Company (*EADS*) France S.A.S. with the University of Technology of Compiegne (*UTC*) as partner. The

simulation can be carried out by means of analytical procedures for simple cases and using the *BEM* for more complex structures. Crack-Kit® can perform two-dimensional analysis in both plane stress or plane strain calculations for any geometry. Multi-site damage can be treated automatically. The tool includes the possibility to analyse contact analysis between several pieces, to evaluate crack initiation under multiaxial fatigue loading and to analyse the propagation of cracks. For this last feature, the crack length or the number of the loading cycle can be automatically controlled. Multi-crack propagation can be computed in an automatic way. It takes into account crack interaction and coalescence. The crack propagation direction is automatically calculated using the maximum shear stress criterion. The available crack propagation laws are Paris and modified Forman law. Furthermore, probabilistic calculations of fatigue crack initiation can be computed based on the Monte-Carlo approach. This program can also treat spectrum-loading [W5].

5.2.5 StressCheck®

StressCheck® is a tool developed by the Engineering Software Research & Development, Inc. (*ESRD*). It is a p-version stress analysis tool in an "easy to use" handbook interface. This handbook interface provides reliable solutions quickly and conveniently for design. StressCheck® can calculate displacements, stress intensity factor, *J*-integral and stress distributions. Furthermore, it has special features to analyse fastened connections, including cold working effects [W6]. However, it does not have the capability to compute automatically crack growth curves, but this can be overcome by means of NASGROW® or AFGROW®. StressCheck is in this case exploited to calculate beta factors, i.e. $f_{ij}^{I}(\varphi)$, $f_{ij}^{II}(\varphi)$ and/or $f_{ij}^{III}(\varphi)$ in equation 2.2.1 for different crack lengths. For example, in a middle tension specimen loaded under pure tension, (pure *Mode I*), σ_{xx} and $f_{xx}^{I}(\varphi)$ are calculated from the computed *SIF*-values, K_I, along the growing crack, *2a*, using the following equation:

$$f_{xx}^{I}(\varphi) = \frac{K_I}{\sigma_{xx}\sqrt{2\pi a}} \quad (5.1)$$

The crack growth curves are then generated with the analytical code by means of the beta factors.

5.3 Tested tools

First of all a pre-selection was carried out based on the tool-descriptions and their accessibility. Finally, only two tools were deeply analysed.

5.3.1 First selection

The analytical codes (NASGRO® and AFGROW®) were discarded due to the disadvantage that only simple predefined specimen geometries can be used. Nevertheless, these tools can be used to complement non-analytical codes for other applications as those searched in this investigation.

Although both SAMCEF® and ABAQUS® have the capability to compute the *SIF*s in all three modes of loading, they were discarded because other tools representative of the *FE*-method had better accessibility at *EADS* Group, i.e. ANSYS® and StressCheck®. Moreover, ABAQUS® is a tool that could not be qualified as "easy to use" compared with the other software.

BEASY® was leftover due to the fact that the solutions for the crack propagation simulation had shortly appeared and it was still on development stage and test phase (stand on summer 2002).

On the other hand, ANSYS®, FRANC3D®, Crack-Kit® and StressCheck® were selected. The first was selected because it is available at *EADS* Deutschland GmbH, the second is free of charges and can be downloaded from Internet. Crack-Kit® was selected because it was developed inside the *EADS* group, and StressCheck® was selected after being proposed by Airbus design department, which facilitated and supported its use and test.

In order to be able to evaluate these tools, a familiarisation process was necessary. During this process several problems were found and, in the development of the work trying to solve them, the real capabilities of the software were better understood.

The extraction of K_{II} in *2D*, K_I and K_{II} in *3D* with ANSYS® could only be done using programming capabilities and defining "manually" special *3D*-elements at the crack tip. In other words, they could not be computed in a direct way without previous knowledge on ANSYS® programming language. This means that this program cannot be evaluated as "easy to use". On the other hand, the possibility to define the pre-processing and post-processing on an interface

and thus allowing the definition of geometric parameters as variables or constants, makes this tool to be evaluated positively regarding the searched design facilities. In addition, this interface allows ANSYS® to be directly implemented by the user.

With FRANC3D® the extraction of both K_I and K_{II} as well as the *T*-stress on *2D*- and *3D*-models are supported. Crack growth laws, crack turning criteria based on second order theories, and crack closure laws are already available in the program. On the other hand, the generation of a model is costly and difficult to be updated, which makes it not suitable for design. This fact, added to the difficulties to extract accurately the desired information avoided to define this tool as "easy to use". The mechanical properties can be edited, but the tool does not support the edition of crack growth parameters. However, Cornell University offers the possibility to perform such material implementations via a cooperation agreement.

Crack-Kit® does not have the capability to extract fracture mechanics parameters on *3D*-models. However, the cost of time to be familiarised with is low and it has the skills to easily create meshes, enter material properties and boundary conditions. In other words, it is "easy to use". Beside this, each individual element or object can be easily edited, therefore it can be considered with design facilities. Although the boundary conditions are easily created and edited, they are limited, and it is not possible to implement the tool directly by the user.

The calculation of the *SIF* under *Mode I* and *II* for *2D*- and *3D*-models is possible by means of StressCheck®. Meshes can be automatically or manually produced. Increasing the p-element order allows a quick check on the convergence of the solution. This check informs the user about the minimal p-element to be used and about the necessity to create a finer mesh in order to obtain convergent results. Its window menu function allows entering material properties and boundary conditions in an easy way. Moreover, its handbook interface allows parameterising the geometry, the material properties and the value for the boundary conditions. This ability is very important and useful for design studies. The implementation is possible by means of an interface, but an arrangement should be taken with the developing company.

Table 5.1 summarises the advantages and drawbacks found for the four selected tools.

As it can be seen in Table 5.1, the two best tools congruent with the conditions defined, were FRANC3D® and StressCheck®. Next section delve into the capabilities of these two software by

analysing the *MT*- and the *2SP*-specimens in *3D* for a crack growth on L-T direction and comparing the results with the experimental test data described in section 4.3.

Table 5.1. Tool evaluation

	ANSYS®	***Crack-Kit®***	***FRANC3D®***	***StressCheck®***
K_I and K_{II} on 2D models	Only K_I without programming	++	++	++
K_I and K_{II} on 3D models	Only with programming	-	++	+
Familiarisation process	-	++	+	++
"Easy to use"	-	+	-	++
Design facilities	+	+	-	++
Implementation	++	-	-	+
Positive remarks	* Large number of users	* Developed at *EADS* * *2D* crack path prediction capability	* *2D*/*3D* crack path prediction capability * *T*-stress criterion	* *2D* crack path prediction capability

5.3.2 Working with FRANC3D®

FRANC3D® can view already existent geometry models, attach material properties and boundary conditions, mesh the surfaces, create an initial flaw, perform the boundary element stress analysis, read and display the results, propagate the crack, and rebuild the mesh for subsequent analyses, but it does not create new geometry models [94].

However, within the FRANC3D program pack, there is a second program called the Object Solid Modeller (*OSM*) that has an environment similar to that of FRANC3D® (similar modelling window, view control, menu system and dialog boxes). The initial geometry model can be created by means of this program or by transforming the data from other solid modelling/design program into a format that FRANC3D® can read.

Taking profit from one of the two symmetry axis (vertical), a *3D* half model of the *MT*- and *2SP*-specimen were generated by means of ANSYS® with a quite coarse mesh. The models were then read with the *OSM* program and they were converted to a format compatible with FRANC3D® according to [95]. Figure 5.1.a illustrates the created and converted model in the case of the *MT*-specimen. A full *3D*-model of the *2SP*-specimen was also modelled in order to analyse the performance of FRANC3D® to calculate more complex structures and to perform multi-crack propagation analysis.

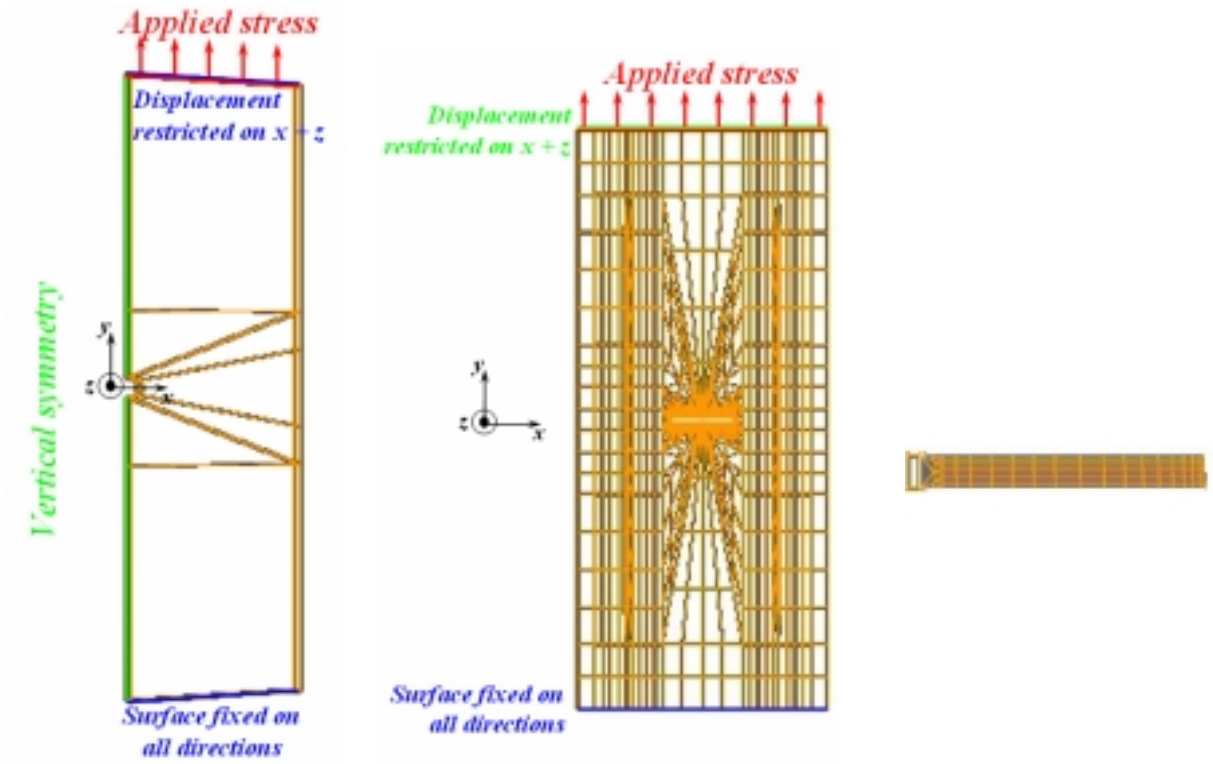

a) *b)* *c)*

Figure 5.1. a) MT-geometry model after being treated with OSM, b) 2SP full-meshed model after automatic crack propagation, c) crack mesh after 16 steps of automatic propagation

Conventional *FE*- or *BE*-tools associate all attributes (material properties and boundary conditions) with the mesh of the numerical model. In FRANC3D®, all attributes are associated with topological entities. The boundary conditions are associated with faces, material properties with regions, and displacements with vertices and edges. The topology has a second role operating as an organizing schema for the storage of analysis attributes.

For the half *MT*- and *2SP*-specimen, a symmetry condition at the specimen load centre-line was assigned. This condition is equivalent to set the normal displacement component to zero. In all models (half *MT*, half *2SP* and complete *2SP*), the bottom face of the models was fixed in the lateral and vertical directions and the upper face was fixed in the lateral directions. A traction stress of *100* MPa (and *180* MPa in a second run analysis) was imposed perpendicular to the upper face for the *MT*-models and *100* MPa for the *2SP*-models. All regions were assigned with the elastic isotropic behaviour of the alloy 6013-T3 with the values obtained on the performed tensile and residual strength tests in L- and LT-directions, respectively.

Table 5.2. Standard elastic isotropic material properties of the AA 6013-T3 in L-direction

Young's modulus [MPa]	*Poisson's ratio [-]*	*Fracture toughness [MPa*m$^{1/2}$]*	*Density [g/cm^3]*
68500	0.33	46	2.71

The initial geometry models were discretised by subdividing manually the existing edges and using the automatic mesh algorithm. A first analysis without any crack was performed to ensure that all boundary conditions and material properties were assigned correctly. Afterwards, through the thickness cracks with initial length of *2.5* mm were put manually in the centre line of the modelled specimen starting on the half-circle with *0.5* mm radius. This location corresponds to the point "C" for the *MT*-specimen depicted in Figure 5.2.a. The cracks were all meshed by subdividing the crack face and mapped bilinear in order to have relatively many and well shaped elements (quasi-square) to achieve sufficient degree of accuracy on the analysis as illustrated in Figure 5.2.b for the *MT*-specimen. The portion of the geometry model that was affected by the crack operations loosed its previous mesh and subdivisions information. In this occasion, this zone was automatically re-meshed. Examples of the resulting mesh are illustrated in Figure 5.1.b and c for the *2SP* and in Figure 5.2.c for the *MT*-specimen.

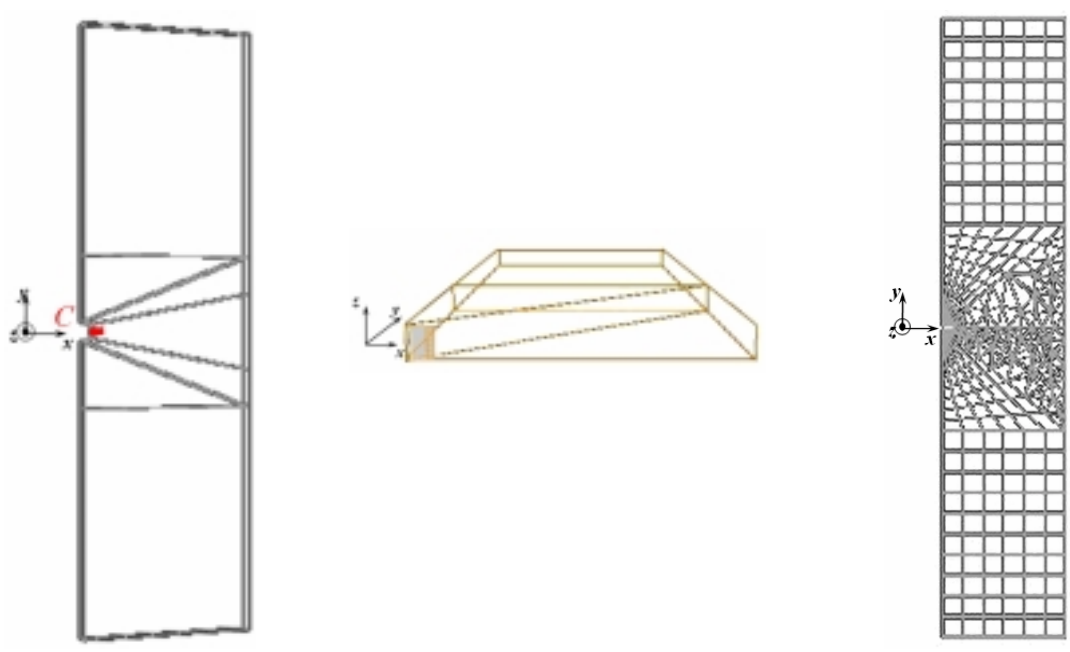

a) ***b)*** ***c)***

Figure 5.2. a) Application point (C) of the through crack, b) bilinear mapping of the crack and c)automatic re-meshing for the MT-specimen

The fracture of the cracked models was then fracture-analysed extracting the *SIF* for the crack front when the simulation run finished. The determination of the new crack front was done by

means of the extracted *SIF*. The point in the crack front with the maximal *SIF* was advanced with the user defined extension. The amount of crack growth for the other points is based on the ratio SIF/SIF_{max}. The first crack front advance was performed in a semi-automatic way according to [95]. The crack extension was *1.5* mm. From this state, crack propagation analyses with a crack extension of *1.5* mm until a maximal crack length of *27.5* mm were carried out automatically governed by the Paris regime.

Table 5.3. Paris constants

	Thickness [mm]	C_p	n_p
L-T	1.6	7.3×10^{-8}	3.03
	2.5	1.5×10^{-7}	2.80
45º	1.6	1.7×10^{-8}	3.39
	2.5	8.6×10^{-8}	2.87
T-L	1.6	1.4×10^{-7}	2.77
	2.5	1.5×10^{-7}	2.79

The introduced Paris constants, C_p and n_p, were found out by means of curve fitting on the log-log plot of *da/dN* vs. *ΔK* curves, as illustrated in Figure 5.3, which were obtained from the crack growth rate test results on the *MT*-specimens (set reference DE02).

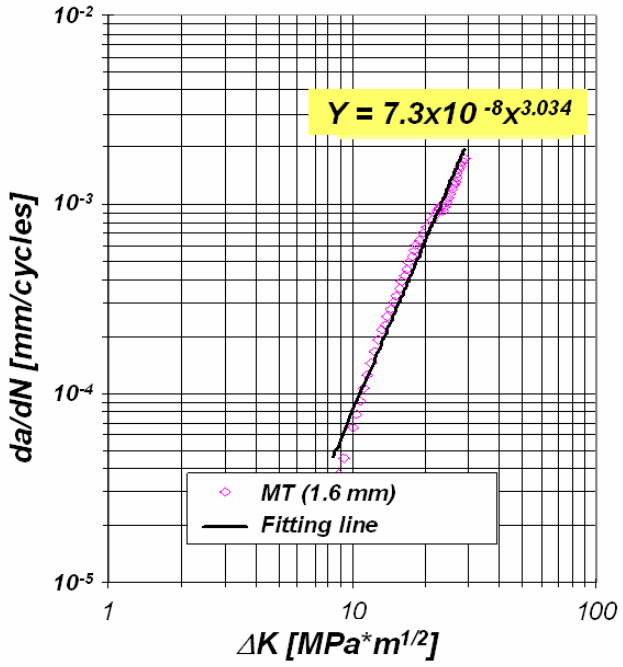

Figure 5.3. Extraction of the Paris constants from the crack growth rate results for the MT-specimens loaded with 100 and 180 MPa in L-T direction. Specimen thickness = 1.6 mm

The simulation of the crack propagation was conducted until the maximal crack propagation extension or the fracture toughness was achieved. The life of the specimen was calculated

introducing a straight line on the crack face as depicted in Figure 5.4. At each interception line-crack front, the stress intensity factor was automatically determined and the life of the specimen was found out by adding the life between successive crack front positions.

Figure 5.4. Illustration of the analysis line (here red) for the extraction of the fracture mechanics parameters. Every orange line defines a crack front. In this case there are 17 crack fronts

The number of elements produced on these crack propagation simulations are summarised on Table 5.4.

Table 5.4. Number of elements for the meshed models in FRANC3D®

	Number of elements (approximately)	
	Initial crack	***Propagated crack***
Half MT-models	740	2200
Half 2SP-models	1000	2500
Full 2SP-model	3150	5200

The assessment of crack propagation on the *MT*-specimen governed by the Paris crack growth regime was satisfactory, as can be seen in Figures 5.5.a and b where the results of simulations are compared with experimental results.

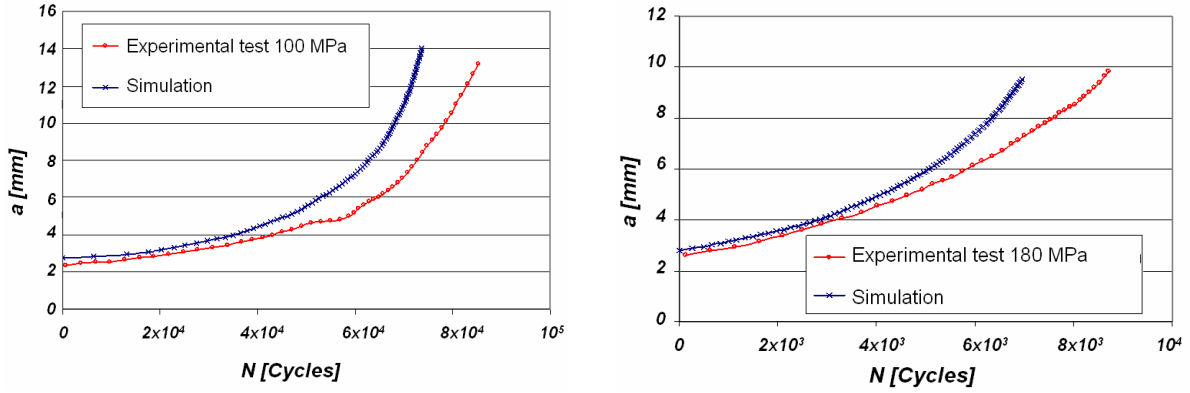

a) ***b)***

Figure 5.5. Test and simulation of the MT-specimen with a thickness of 1.6 mm and an upper stress of a) 100 MPa and b) 180 MPa

However, the assessment on the *2SP*-specimen was not satisfactory. An attempt to improve this was done by trying to use the Forman-Newman-deKonning (*FNK*) instead of the Paris law, but

in this case the available databank did not contain the material parameters for the alloy *AA* 6013-T6 and new parameter-values could not be introduced. The parameters for the aluminium alloy 7475-T7351 were used instead to analyse FRANC3D® further.

During the simulation of the *2SP*-specimen other problems appeared. First, it was observed that the crack growth results were not reproducible. Secondly, the crack growth analysis of the full model using the existing automatic crack path did not produce reliable results, specifically the program simulated an anti-symmetric effect on the symmetric *2SP*-specimenas illustrated in Figure 5.6, which was not observed during testing.

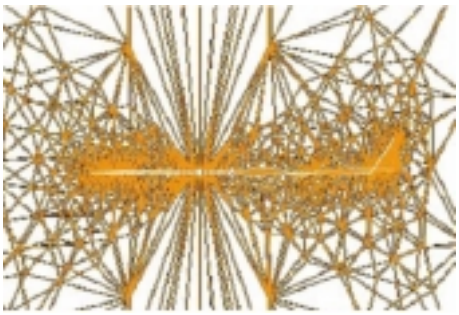

Figure 5.6. Crack propagation on the 2SP using the full model and the crack turning capability

In order to solve these problems and implement other models and tool abilities, the code developer (Cornell University) was contacted and the possibility to create cooperation was checked. Unfortunately, the needed performance could not be afforded at that moment.

5.3.3 Working with StressCheck®

Solid geometries constructed with *CATIA* or Computer Aided Design (*CAD*) Systems can be imported to StressCheck®, where they must be modified through the addition of new solid objects and the application of Boolean or blend operations. StressCheck® also includes a "Parasolid" geometric facility to create directly the desired solid, where all objects may be created in parametric form [96].

Taking profit from the two symmetry axis (horizontal and vertical) of the *MT*-specimen and one of the two symmetry axis of the *2SP*-specimen, a quarter and half *3D*-model, respectively, were generated with StressCheck®. All geometric dimensions and mesh parameters concerning the crack were created in parametric form. A full *3D*-model of the *2SP*-specimen including the

clamping device was also modelled in order to analyse the performance in calculating more complex structures.

Meshes are usually attached to geometric objects, which are defined parametrically, obtaining indirectly a parameterised mesh. Nodes were manually defined along the geometric model depending on the desired final mesh. Elements were constructed by selecting these nodes.

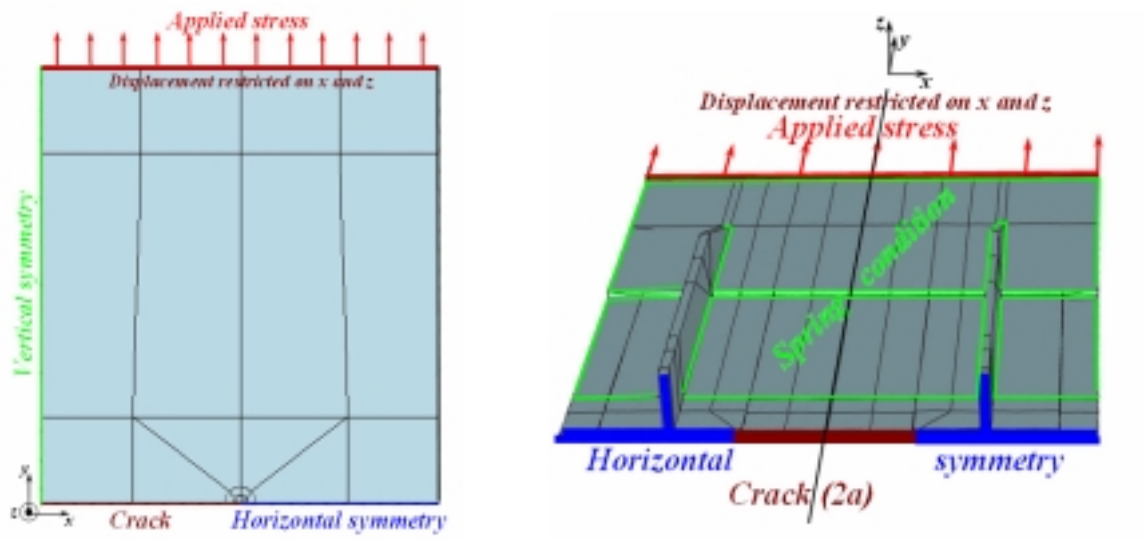

a) ***b)***

Figure 5.7. Mesh and boundary conditions for a) quarter MT-model and b) half 2SP-model with StressCheck

For the quarter *MT*-specimen, symmetry conditions were assigned at the vertical and horizontal centre-lines. These symmetry conditions were not applied at the crack surface, as represented in Figure 5.7.a. For the half *2SP*-model, symmetric conditions were applied partially on the horizontal centre-line, as illustrated in Figure 5.7.b. The upper faces of these models (quarter *MT* and half *2SP*) were fixed in the *x*- and the *z*-directions. The upper holes of the clamping device on the full *2SP*-model were also fixed in the *x*- and the *z*-directions. For the *2SP*-model a spring coefficient condition with a value of *50* N/mm was applied normal to the front and back of the specimen in order to model the boundary condition generated by the anti-buckling device. These surfaces are defined by green lines in Figures 5.7.b and 5.8. The bottom hole-surfaces of the clamping device, Figure 5.8, were fixed in all directions.

A traction stress of *100* MPa (and *180* MPa in a second run analysis) was imposed perpendicular to the upper face for the *MT*-model and *100* MPa for the half *2SP*-model. On the full *2SP* model, a *100* MPa stress was applied in form of a bearing stress at the upper hole of the clamping

device. The bearing stress is simulated as a sinusoidal traction around the hole, which approximates the interaction of the pin with the clamping device.

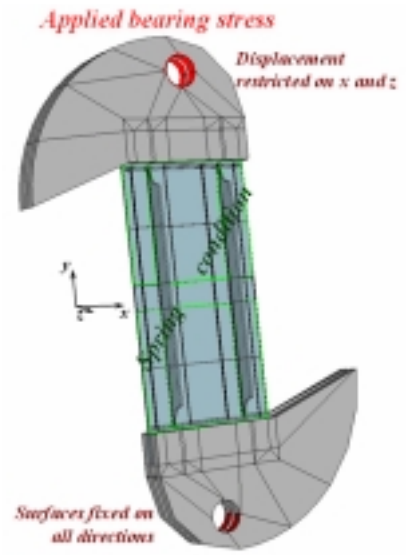

Figure 5.8. Mesh and boundary conditions for the full 2SP-model without crack modelled with StressCheck

All regions were assigned with the elastic isotropic behaviour of the *AA* 6013-T3 with the values of the mechanical properties given in Table 5.2. First simulations were performed using polynomials of degree from 5 to 8 in order to check the convergence of the solution and the quality of the mesh. Further analyses were performed with a polynomial degree equal to 8.

The cracked models were fracture-analysed extracting the *SIF* for different crack lengths by means of an automatic parametric change on the value of the crack length and the local mesh around the crack. The radii of the path-integral to compute the *SIF* were selected to be situated on the second element circle around the crack tip, as illustrated in Figure 5.9, in order to avoid oscillations on the results.

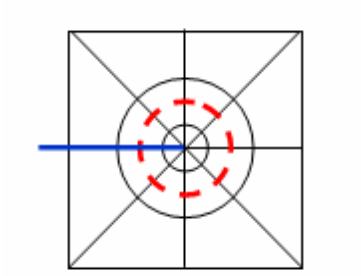

Figure 5.9. Crack tip mesh illustrating the path-integral (hatched contour)

Crack growth rate curves were determined for the *MT*-specimens by means of the Paris regime and its correspondent constants summarised in Table 5.3. Figure 5.10 illustrates the simulation results compared with experimental results on the *MT*-specimen.

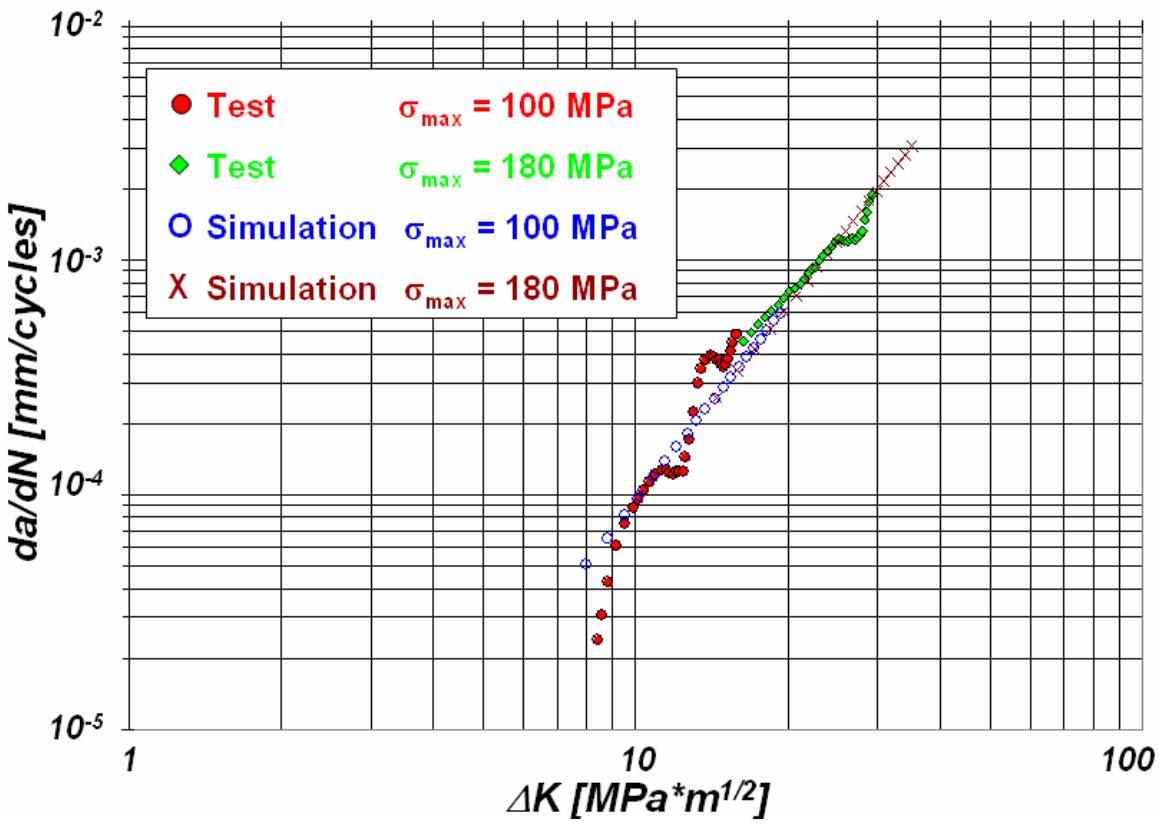

Figure 5.10. Experimental test and simulation results for the MT-specimen with a thickness of 2.5 mm

The experimental curve of testing, *da/dN vs. 2a*, depicted in Figure 5.12 was calculated by means of the Forman law together with the fracture toughness value given in Table 5.2 and the parameters $C_f = 3.42x10^{-5}$ and $n_f = 1.96$ found out by means of a curve fitting on the log-log plot of $(da/dN)x(1-R)k_c$-ΔK vs. ΔK curves obtained during testing of the *MT*-specimen. Table 5.5 summarise the obtained constants for the different thicknesses and directions.

Table 5.5. Forman constants

	Thickness [mm]	C_f	n_f
L-T	1.6	$1.56x10^{-5}$	2.22
	2.5	$3.42x10^{-5}$	1.96
45º	1.6	$3.47x10^{-6}$	2.60
	2.5	$1.11x10^{-5}$	2.25
T-L	1.6	$3.50x10^{-5}$	1.91
	2.5	$3.41x10^{-5}$	1.96

Two different models were used for the simulation of the half *2SP*-specimen; the first one takes into account the crack propagation on the skin and the second the growth of the crack on the outer flange, as illustrated in Figure 5.11.

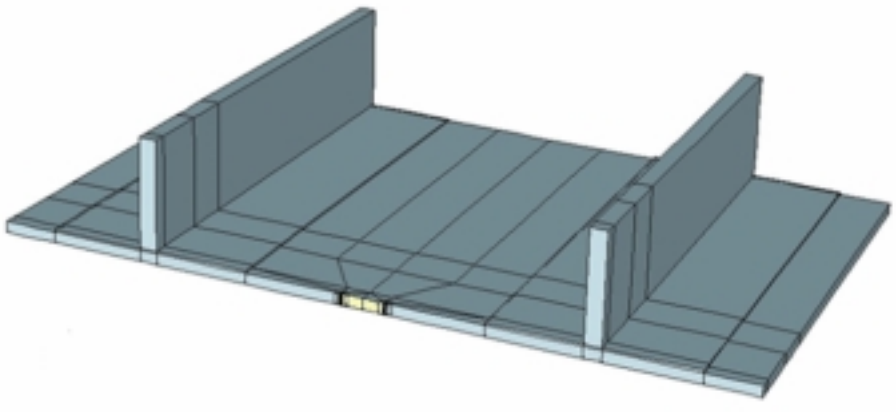

a)

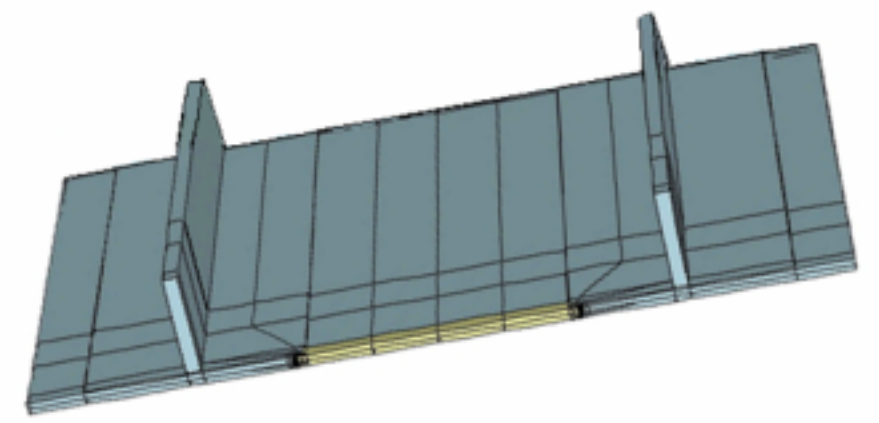

b)

Figure 5.11. Models for the 2SP-specimen a) with the crack in the skin and b) in the outer flange

As it can be seen in Figure 5.12, the *FE*-results show correspondence with experimental results, using the material data from simple standard specimens, i.e. *MT*-specimens. The gap in the diagram at a crack length of *54* mm appears because there is a change in the thickness at this point and the *SIF*-calculation at a thickness step is theoretically not defined. Although the propagation of the crack tips in the simulations was performed assuming symmetrical crack growth, the crack propagation in the actual test occurred asymmetrically. One crack tip propagated faster than the other.

Therefore, in the experimental test, one of the stringers was reached faster than in the simulation, producing an early reduction of the crack growth rate as it can be seen for larger crack lengths in

Figure 5.12. Moreover, the difference of crack growth rate reduction between the experimental results and the simulation is generated because the model did not include the fillet between the skin and the stringer, i.e. there is a stress concentration which increases the *SIF* [82].

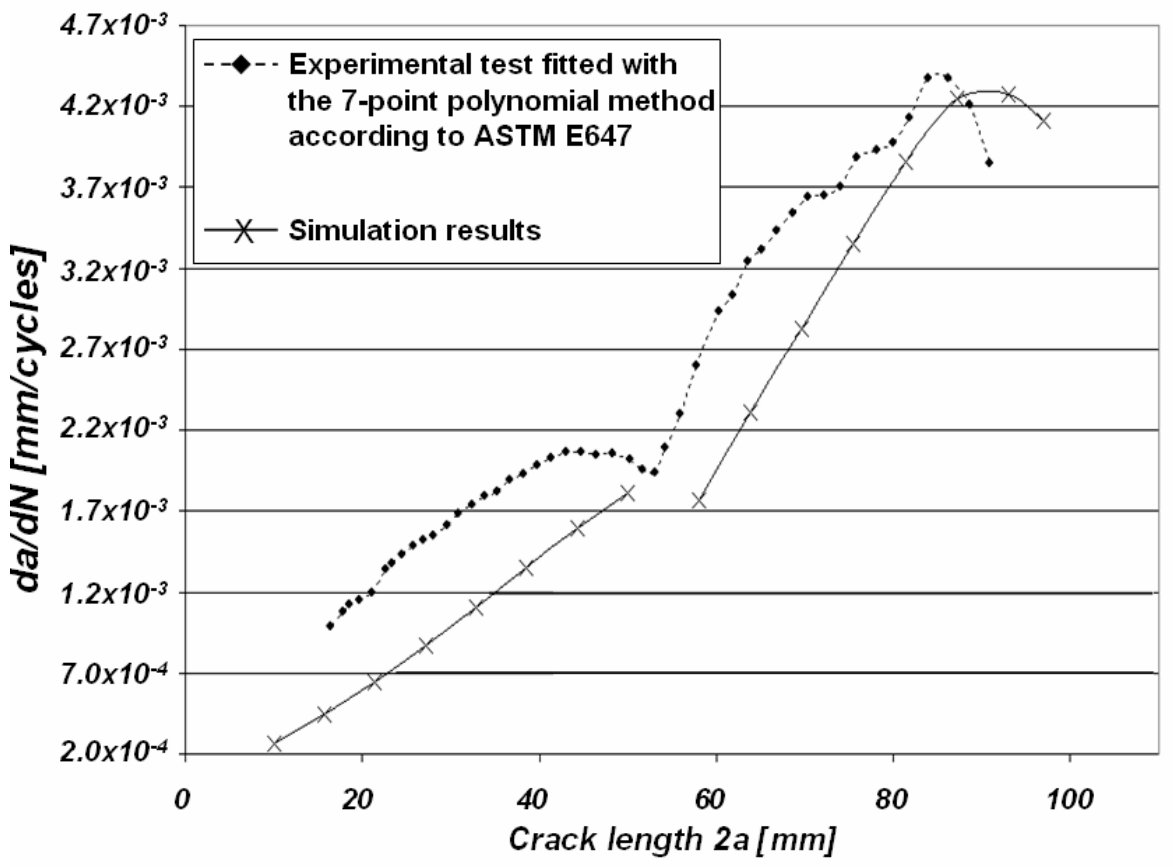

Figure 5.12. Experimental test and simulation results for the half 2SP-specimen

The number of elements produced for these crack propagation simulations are summarised in Table 5.6.

Table 5.6. Number of elements for the meshed models in StressCheck®

	Number of elements	
	Crack on the skin	***Crack on the outer flange***
Quarter MT-model	22	-
Half 2SP-model	242	274
Full 2SP-model	558	-

The crack propagation predictions on the *MT*- and *2SP*-specimens by means of the Paris and Forman regimes were satisfactory. Furthermore, the results obtained with the full *2SP*-model were reproducible, they took only half hour of computation time and they had less than a *2*% deviation as compared with the results on the half model.

5.3.4 Conclusion of the tool analyses

As demonstrated in sections 5.3.2 and 5.3.3 both tools are adequate to perform crack growth assessments. StressCheck® was found to be more friendly (easy to use, parametric model, p-element, etc.) and also lower computing time was needed, as overviewed in Table 5.7. It was then decided to select StressCheck® to perform crack turning assessment analyses.

Table 5.7. Comparison between StressCheck® and FRANC3D®

		StressCheck®	***FRANC3D®***
Time for the full 2SP-model		0.5 h	40 h
Problems with calculations		No one	Some
Exactness		Dependent on crack length	
Crack direction	***2D***	Assessed after the maximal principal stress criterion	Assessed with the *T*-stress criterion
	3D	Shall be pre-defined	Assessed (variably)
Reproduction		O.K.	Badly
K_I		Comparable	
K_{II}		1 point	Number variable of points
K_{III}		--	Number variable of points
Crack bifurcation		Possible defining different cracks	Manually feasible
Support		Good	No commercial software
Application		Elastic-plastic, fracture mechanics, crack rotation in *2D*-models, and K_I, or K_{II}-calculations	Cyclic crack propagation
Problems		Small, local plastic deformation	Large structures simulation, *3D* crack path propagation
Qualities		p-elements: relation elements/thickness > 1:200	Crack bifurcation for solid and rotation
Development		Feasible	Not immediately possible

5.4 Implementation of the tool

StressCheck® must be implemented with the capability to extract the *T*-stress parameter to perform crack turning analyses under *Mode I* conditions. The computation of the *T*-stresses can be achieved by means of the stress substitution method, the second order weight function method, the Leevers & Radon variation method, the interaction integral method, the line spring method or using path independent integrals [33]. This last procedure is based on Eshelby's energy momentum tensor or on the Betti-Rayleig reciprocal theorem [49]. More information on these methods can be found on references [37, 57, 97, 98].

After reviewing the best and more used *T*-stress methods in the literature, *ESRD* Inc. was contacted in order to decide which was more adequate for StressCheck®. The implementation task was carried out by *ESRD* Inc. under assignment of *EADS* Deutschland GmbH and Airbus

Deutschland GmbH. The computation of the *T*-stress was implemented within the fracture module of StressCheck® as a post-processing operation based on the Betti-Rayleigh reciprocal theorem.

On a hyperelastic body subjected to two systems of body and surface forces, the Betti-Rayleigh reciprocal theorem states that the work done by a first system in a displacement, *u*, caused by a second system, is equal to the work done by the second system in the displacement, *u*, caused by the first. This is expressed in equation 5.4.1 where the body forces *f* and f^* and the surface tractions t_i and t_i^* produce the displacements u_i and u_i^*. The symbol * describes the calculated force, traction or displacement functions in the local Cartesian coordinate system at the crack tip.

$$\iint_A t_i^* u_i dA + \iiint_V f_i^* u_i dV = \iint_A t_i u_i^* dA + \iiint_V f_i u_i^* dV \qquad \textbf{(5.4.1)}$$

For *2D*-cases without body forces and assuming that the total strain energy needs to be bounded at the crack tip, the extraction of *T*-stress contributions without the contributions from the singular and other higher order terms is computed by *FEA* according to [49] by the following contour integral:

$$T = \tilde{E} \oint_{C_e} \left(\sigma_{ij}^* u_i^{FE} - \sigma_{ij}^{FE} u_i^* \right) n_j dC = \tilde{E} \left[\oint_{C_e} \left(T_x^* u_x^{FE} + T_y^* u_y^{FE} \right) r d\varphi - \oint_{C_e} \left(T_x^{FE} u_x^* + T_y^{FE} u_y^* \right) r d\varphi \right] \qquad \textbf{(5.4.2)}$$

From Figure 5.13 it can be seen that n_i ($i = 1, 2$) are the components of the outer normal to the integration path. The calculated stress functions (σ_x^*, σ_y^* and τ_{xy}^*) at the crack tip can be written as $\sigma_x^* = (\cos 2\varphi + \cos 4\varphi)(2\pi r^2)^{-1}$ ***(5.4.3.a)***, $\sigma_y^* = (\cos 2\varphi - \cos 4\varphi)(2\pi r^2)^{-1}$ ***(5.4.3.b)*** and $\tau_{xy}^* = (\sin 4\varphi)(2\pi r^2)^{-1}$ ***(5.4.3.c)***. The calculated displacement functions (u_x^* and u_y^*) in the same coordinate system are given by:

$$u_x^* = -\frac{\kappa \cos\varphi + \cos 3\varphi}{8\pi G r} \qquad \textbf{(5.4.4.a)} \qquad u_y^* = \frac{\kappa \sin\varphi - \sin 3\varphi}{8\pi G r} \qquad \textbf{(5.4.4.b)}$$

where $\kappa = \kappa_1 = (3\text{-}4\nu)$ and $\tilde{E} = E_1 = E/(1-\nu^2)$ for plane strain and $\kappa = \kappa_1 = (3\text{-}\nu)/(1+\nu)$ and $\tilde{E} = E_2 = E$ for plane stress, with ν and E being the Poisson's ratio and the Young modulus of

the material, respectively. σ_{ij}^{FE} and u_{ij}^{FE} are the stresses and displacements on Γ obtained from the finite element solution.

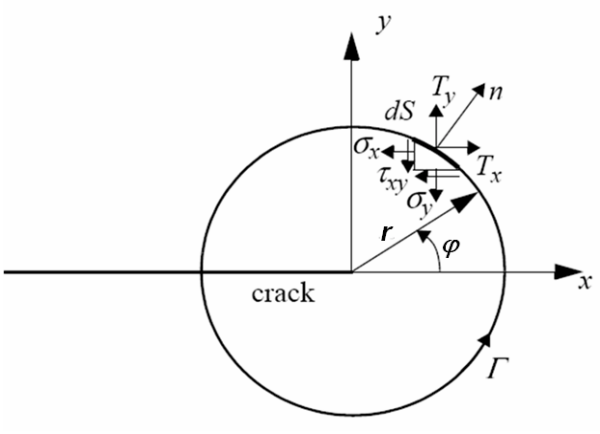

Figure 5.13. Contour integral near the crack tip [99]

In three-dimensions, the *T*-stress is computed using the same path-independent integral over a circular path, Γ, around the crack front at a selected point. In other words, the process determines a plane, which is normal to the crack edge and tangent to the selected point. The global components of stresses and displacements along the circular path contained in this plane are calculated. These stresses and displacements are then integrated with the calculated functions described above to compute the *T*-stress.

5.5 Reliability of the tool

The reliability of the tool for stress analysis and especially for *SIF* on small and more complex structures has already been demonstrated in the simulation of the *MT*- and *2SP*-specimens, as illustrated in Figures 5.10 and 5.12.

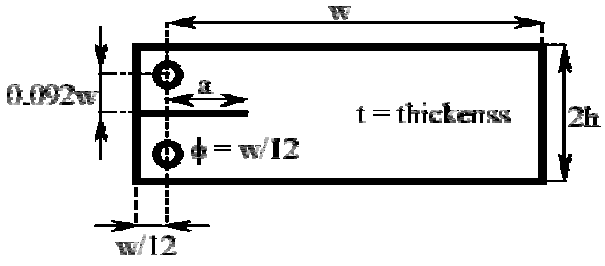

Figure 5.14. DCB-specimen dimensions [9]

The evaluation of the reliability of the implemented extraction capability took place by means of comparing analytical, simulation and literature results on the *DCB*-specimen. The geometry and dimensions of the analysed *DCB*-specimen are shown in Figure 5.14.

5.5.1 Theoretical Stress Intensity Factor calculation

General analytical equations from the literature to evaluate the *SIF* for the *DCB*-specimen depicted in Figure 5.14 are equations 5.5.1 and 5.5.2 for large and small *a/h* ratios, respectively.

$$K = \frac{F}{t}\sqrt{\frac{12}{h}}\left(\frac{a}{h}\right) \quad \textbf{(5.5.1)} \qquad K = \frac{F}{t}\sqrt{\frac{2}{\pi a}} \quad \textbf{(5.5.2)}$$

where *F* is the applied load, *2h* is the height of the specimen and *a* is the crack length.

Based on the results from Gross and Srawley [100], who used the beam solution extended to small values of *a/h*, the stress intensity factor for the *DCB*-specimen can be calculated using equation 5.5.3.

$$K = \frac{F}{t}\sqrt{\frac{12}{h}}\left(\frac{a}{h} + 0.687\right) \quad \textbf{(5.5.3)}$$

Equation 5.5.3 should not be used for crack lengths larger than *w*-2*h* to avoid the influence of the edge of the specimen [9, 23].

Other expressions have been also proposed for the *SIF* of the *DCB*-specimen. Thus, Fichter [101] found an equation to calculate the *SIF* based on the Wiene-Hopf technique [102], which is valid for *a/h* ratios greater than *2* and it is given by:

$$K = \frac{F}{t}\sqrt{\frac{12}{h}}\left(\frac{a}{h} + 0.6728 + 0.0377\left(\frac{h}{a}\right)^2\right) \quad \textbf{(5.5.4)}$$

On the other hand, Foot et al. [103] developed an explicit solution valid for all *a/h* ratios with *(w-a)/h > 2*, where *w* is the width of the specimen from the line where the force *F* is applied, which can be written as,

$$\frac{Kt\sqrt{h}}{F} = \sqrt{12}\left(\frac{a}{h} + 0.673\right) + \sqrt{\frac{2h}{\pi a}} - \left(0.815\left(\frac{a}{h}\right)^{0.619} + 0.429\right)^{-1} \qquad \textbf{(5.5.5)}$$

5.5.2 Simulation results

A full *3D*-model of the *DCB*-specimen was generated with StressCheck®. All geometric dimensions and mesh parameters were created in parametric form. The dimension ratios of the model are selected according to the literature [8, 49, 53, 98, 103] to be *a/w = 0.5* and *h/w = 0.2*. The two upper and bottom nodes at the end of the specimen were fixed in the *y*- and the *z*-directions and the two middle nodes at the end of the specimen were fixed in the *x*-direction. A traction stress of *100* MPa was applied in form of a bearing stress at the upper and lower hole of the specimen. The bearing stress was selected because it represents the interaction of the pin with the hole better than an applied point force condition, i.e. it eliminates any influence of perturbations from the point force load. Figure 5.15 presents the mesh and the boundary conditions for the *DCB*-model.

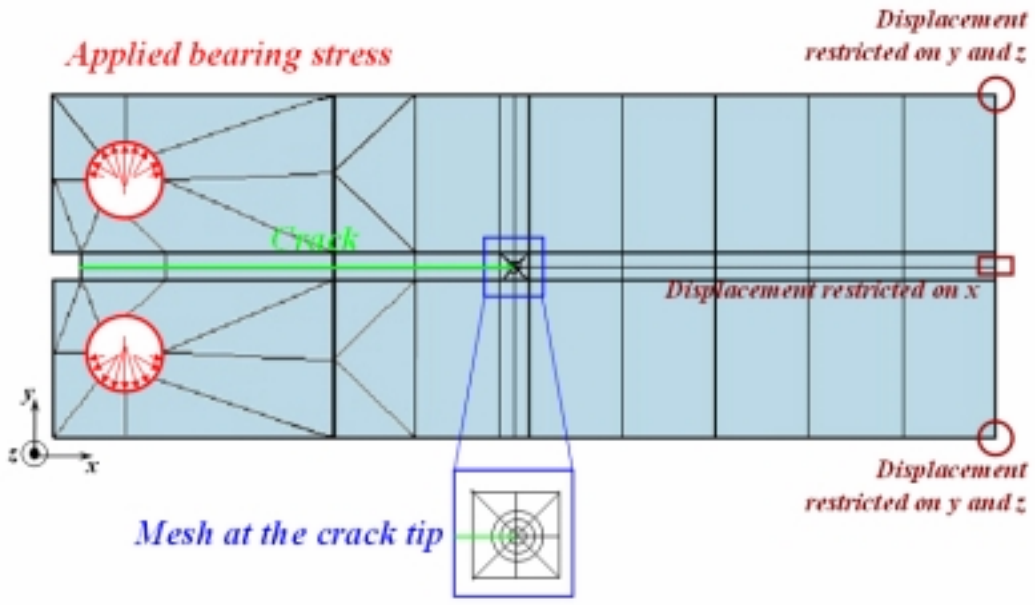

Figure 5.15. Boundary conditions and mesh from the simulated DCB-specimen

All regions were assigned with the elastic isotropic behaviour of the *AA* 2024-T3 with the values given in Table 4.5. First simulations were performed with polynomials with degrees from 5 to 8

in order to check the convergence of the solution and the quality of the mesh. The number of elements was *90* on this simulation analysis.

Numerical experiments showed that it was not possible to compute the *SIF* and *T*-stresses in a reliable manner inside the elements which contained the crack tip because the solution oscillates. Therefore all the radii of the path-integral to compute both *SIF* and/or *T*-stresses were selected to be situated in the second or third element circle around the crack tip.

The obtained fracture parameters are summarised in Table 5.8 for p-element order equal to 8 with a linear (*LA*) and a geometric non-linear analysis (*NLA*). A geometric non-linear analysis has to be applied when the structure experiences large deformations, i.e. large displacements and/or rotations. The most important feature of geometric non-linear analysis is the fact that loads, defined in a normal/tangent reference frame, will remain normal/tangent throughout the deformation.

Table 5.8. StressCheck results for the DCB-specimen with a/w = 0.5; h/w = 0.2

p = 8	***K_I [MPa*m$^{1/2}$]***	***K_{II} [MPa*m$^{1/2}$]***	***T-Stress [MPa]***
LA	44.52	0.00	187.10
NLA	44.49	0.00	189.80

Table 5.9 contains the fracture values in a normalised form calculated by different authors and the values included in Table 5.8 also normalised.

Table 5.9. Computed values of K_I, T and B for DCB-specimen

DCB (a/w=0.5, h/w=0.2)			
Sources	***$K_I/\sigma(\pi a)^{1/2}$***	***T/σ***	***$B=T(\pi a)^{1/2}/K_I$***
Leevers and Radon (1982) [55]	-	-	2.942
Cardew et al. (1985) [103]	-	-	2.829
Kfouri (1986) [49]	-	-	2.956
Fett (1998) [97]	3.9307	11.5304	2.933
Chen et al. (2001) (p = 11) [8]	3.9225	11.5745	2.9508
Llopart (p = 8 LA)	3.9239	11.4131	2.9086
Llopart (p = 8 NLA)	3.9212	11.5778	2.9526

The defined dimensions for the *DCB*-specimen verify the conditions of validity for equations 5.5.3 to 5.5.5, i.e. *a/h = 2.25 > 2* and *(w-a)/h = 2.75 > 2*. The analytical results for the *SIF* calculated with these equations are:

Table 5.10. Theoretical Value of the SIF on the analysed DCB-geometry

	$K_I/\sigma(\pi a)^{1/2}$	*Equation*
Gross and Srawley [100]	3.9394	(5.5.3)
Fichter [101]	3.9405	(5.5.4)
Foot [103]	4.1006	(5.5.5)

It is obvious that the *SIF* and the *T*-stress simulation results are comparable with those found on the literature as well as those calculated from the equations. However, it is important to recognise that for this structure a geometric non linear analysis is necessary.

Summarising, throughout this chapter it has been shown that StressCheck® is one of the tools that fulfil all the required skills that were demanded for the tool, i.e. the tool calculates K_I and K_{II} on *2D*- and *3D*-structures, it has design facilities, it is able to be implemented and it is "easy to use". Furthermore, the reliability to analyse complex structures and to compute fracture mechanics parameters, both *SIF* and *T*-stress, was successfully proved. With these results, the first task of this doctoral thesis was finished and StressCheck® was ready to be used on fracture analyses and mainly on crack turning analyses under near *Mode I* loading.